A Damped Double Dipole UHF RFID Antenna with Application to Wireless Chemiresistive Gas Sensing

by

Alexander (Olek) Peraire-Bueno

Submitted to the Department of Mechanical Engineering
in partial fulfillment of the requirements for the degree of

Master of Science in Mechanical Engineering

at the

MASSACHUSETTS INSTITUTE OF TECHNOLOGY

February 2022

Author .....
Department of Mechanical Engineering
January 14, 2022

Certified by .....
A. John Hart
Professor of Mechanical Engineering
Thesis Supervisor

Accepted by .....
Nicolas Hadjiconstantinou
Graduate Officer, Department of Mechanical Engineering

A Damped Double Dipole UHF RFID Antenna with Application to Wireless Chemiresistive Gas Sensing

by

Alexander (Olek) Peraire-Bueno

Submitted to the Department of Mechanical Engineering
on January 14, 2022, in partial fulfillment of the
requirements for the degree of
Master of Science in Mechanical Engineering

Abstract

Ultra High Frequency (UHF) Radio Frequency Identification (RFID) tags provide an inexpensive framework for distributed sensing. Materials such as functionalized carbon nanotubes (CNTs) have been engineered to change in resistance when exposed to a variety of analytes. These materials have been added to RFID tags to create low cost sensors that work at a fixed reader-tag separation distance. This thesis proposes a novel approach to create UHF RFID sensing tags that work independent of distance (within the operating range), and are able to sense changes in resistance of a sensing element with a conductivity similar to that of CNT networks. Simulations of the proposed design show two methods of operation, either by comparing the damping between two resonant peaks, or by shifting the resonant frequency of the RFID tag. The first of the two methods of operation is validated experimentally with surface mount resistors, showing a relative change in τ of 0.2 for a 35% change in resistance of the sensing element. Then, a printing process is developed for liquid inks comprising CNTs, and RFID tags are fabricated with functionalized CNTs as the active elements. The functionalized CNTs exhibit an irreversible 65% change in resistance at 100ppm NH_3, resulting in the tags demonstrating a relative change in τ of 0.5 when exposed to 1000ppm NH_3.

Thesis Supervisor: A. John Hart
Title: Professor of Mechanical Engineering

Acknowledgments

I would like to thank everybody who contributed to this work, especially:

- Professor John Hart, for his insightful guidance, curiosity, and enthusiasm, all of which had a hand in my growth as a researcher.
- The members of the Mechanosynthesis Group, for providing valuable mentorship and help throughout my thesis work.
- The MIT Mechanical Engineering Department and the LMP, for the support that comes from being surrounded by such curious and driven individuals.
- My parents, Jaime and Anna, and my brothers, James and Anton, for their unconditional support, without which this thesis would not have been possible, and my cat Coco, for her inspirational curiosity and untimely distractions.

Contents

List of Figures

List of Tables

Chapter 1

Introduction

Ubiquitous, distributed sensing of chemical and environmental factors could provide high-value information for dynamic and data-driven decision making both locally and across large numbers of sensors. For instance, the detection of volatile organic compounds (VOCs) posing risks to public health [1] or the condition of perishable goods, estimated to cause 30% losses in the US supply chain [2], would both greatly benefit from such gathering of information. Cost-effective and mass-produced sensors that can detect specific chemical compounds, temperature changes, or other stimuli of interest are necessary to realize this vision.

Various materials, including pristine and functionalized carbon nanotubes (CNTs) [3] as well as some conductive polymers such as polypyrrole or polyaniline [4], have been engineered to change properties when exposed to selected environmental factors. For instance, pristine CNTs, and the corresponding CNT networks, exhibit a noticeable change in resistance when exposed to changes in temperature [5]. CNTs have also been polymer-functionalized to change in resistance when exposed to gases such as CO_2 [6].

Implementation of these sensors at large scales requires coupling of the changes in material properties to inexpensive, wireless communication and detection means that can be cost-effectively mass produced. For these reasons, Radio Frequency Identification (RFID) technology is a compelling solution, because RFID tags are already produced at a bulk cost

of only 7–15¢ per tag [7] with prices going down to an estimated 5¢ [8] as widespread adoption continues to grow. Within the different RFID frequency bands, the ultra-high frequency (UHF) passive RFID band (between 902MHz and 928MHz in the US) is an attractive option due to its read range, relatively small tag size, and widespread adoption in commercial settings for item tracking [9].

A UHF RFID system consists of a reader and RFID tags and relies on backscatter to operate. The reader transmits power in the form of electromagnetic waves, which are then received by the tag antenna and used to power an integrated circuit (IC) on the tag. By changing its impedance, the IC changes the reflection of the waves back to the reader, thus communicating information stored on the IC. Other information, however, can also be extracted from the tag by analyzing its frequency response within the designated frequency band.

Yang et al. [10] fabricated a bowtie dipole UHF RFID tag with inkjet printed single-walled CNTs as a load. The CNT material exhibited a change in resistance and thus a change in return signal strength of the tag when exposed to 4% ammonia (NH_3). Similar work is done in [11], using single-walled CNTs to sense changes in ammonia exposure by measuring the turn-on power of the tag. Polymer functionalizations can target a variety of gases including H_2O_2, $C_6H_{10}O$, H_2O or can increase sensitivity to NH_3, and changes in resistance of the functionalized CNT networks can be read through (NFC) RFID tags [12]. Moisture sensors [13] have also been made with RFID tags, varying the tag performance based on the absorption of a liquid into a substrate.

These previous works rely on the principle of sensing the return strength signal integrity (RSSI) of the tag. When the resistance of the sensing element changes, the RSSI correspondingly changes at all frequencies, and this change is seen by the reader. However, a limitation of this approach is that there can not be decoupling of the sensing done by the sensor and the reader-tag separation distance because both can increase or decrease the RSSI over the whole frequency range. Kutty et al. [14] address this issue by adding an on-off switch on the tag. The on-off switch allows the tag to provide a reference response that the sensing

response can then be compared to. A limitation of this approach is that the switch must be flipped by additional external components. A similar approach would be to use two tags, one as a reference and one to sense, but that would result in approximately doubling the cost per sensor.

This thesis presents a new approach to decoupling the sensing from the reader-tag distance while maintaining a design complexity and component count similar to that of existing commercial UHF RFID tags. We propose a novel design for an antenna that transduces a change in resistance of a sensing element to a frequency dependent change in the antenna frequency response. We also demonstrate a proof of concept UHF RFID tag using this design. Using a direct-write printer, the resistance, and sensitivity to NH_3, of functionalized printed CNTs is tested. The printed CNTs are then used with the proposed design to create CNT-based NH_3 sensing UHF RFID tags.

Chapter 2

RFID Antenna Design

The proposed antenna design is based on using sensing elements that are significantly less conductive than the metal that is traditionally used for RFID antennas. Thus, it enables the use of CNT-based sensing elements, which can be functionalized to allow for the selection of chemirestivity in response to various environmental factors. We therefore consider sensing elements with a nominal resistance on the order of 0.1kΩ to 10kΩ for a 1mm wide thin film over a gap of about 1mm. This nominal resistance range was determined from experiments shown later in this thesis. Another goal for the proposed antenna is to be sensitive to changes in the conductivity of the material that remain within an order of magnitude.

Rearranging the Friis transmission equation outlined in [15], we can derive an expression relating the power delivered by the RFID reader, P_r, and the power delivered to the tag IC, P_c,

$$P_r = \frac{4\pi d^2 P_c}{A_e G_r \tau} \ , \tag{2.1}$$

where A_e is the effective tag antenna aperture, d is the reader-tag separation distance, and G_r the reader antenna gain. A critical variable affecting the transfer of power is τ, the transmission coefficient, given by,

$$\tau = \frac{4R_a R_c}{|Z_a + Z_c|^2} \ . \tag{2.2}$$

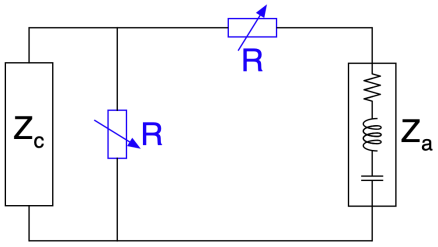

Figure 2-1: Equivalent circuit model of tag, with RLC circuit modeling Z_a

In this equation, R_a, R_c are the resistances of the antenna and the IC, respectively, and Z_a and Z_c are the corresponding impedances. The impedances of the antenna and the chip are perfectly matched when the antenna impedance is equal to the complex conjugate of the chip impedance, $Z_a = Z_c^*$, resulting in $\tau = 1$. We note that in (2.1), d is independent of frequency, whereas τ is dependent on Z_a and Z_c, which in turn are a function of frequency. Therefore, we can decouple changes in the the read power required due to changes in frequency, through τ, and changes in d.

Sensing in the frequency domain, through τ, requires an antenna that will change the imaginary component of its impedance with changes in resistance of the sensing element. Modelling the antenna as an RLC circuit, we can arrange Z_a and Z_c in parallel, as shown in Figure 2-1. A change in resistance for either resistor shown in blue in Figure 2-1 does not affect the circuit's resonant frequency. Consequently, adding a sensing element in series or in parallel with Z_a will not result in a change of resonant frequency.

To produce a frequency dependent change in the frequency response of the tag, a resistive element can be used to split the surface current on the antenna, thus changing a characteristic length of the antenna, influencing its impedance. One way to do this using a conventional RFID tag design is to use the sensing element to change the current path across the meandered dipole section the antenna. This approach, however, requires the current that changes the characteristic length of the dipole to pass through the sensing element. When considering sensing elements with relatively high resistance, this results in severe degradation of tag performance. The tag's response is either insensitive to changes in the sensing element or

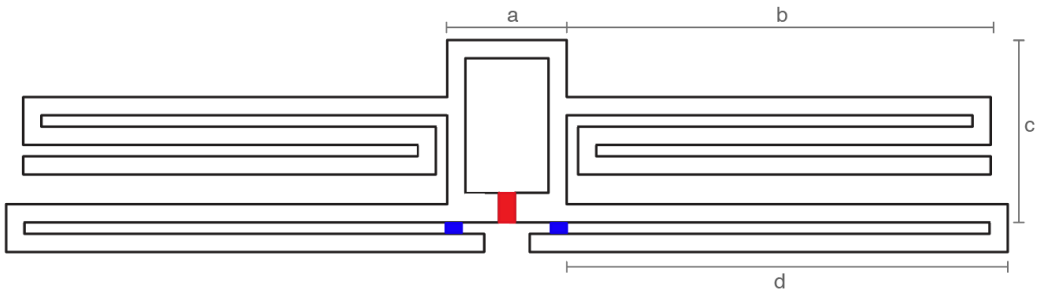

Figure 2-2: Topology of proposed antenna, which includes inductive loop and two sets of dipole arms tuned for different frequencies. The IC is shown in red, and sensing elements are shown in blue.

requires a large amount of current to account for the resistive losses of the sensing element.

The topology used in this thesis, shown in Figure 2-2, addresses both the issues of sensing in the frequency domain and maintaining tag performance. By using two sets of dipole arms, one of the dipoles can be used as a reference while the other varies in τ as the sensing element changes in resistance.

The design process for this topology is similar to that used for conventional commercially available tags [16]. The inductive loop is first designed to impedance match the capacitive impedance of the IC. The dipole arms are then designed to radiate at the desired frequencies and are meandered to reduce the footprint of the tag. In the proposed topology, two sets of dipole arms are added to the tag, radiating at slightly different frequencies around the desired frequency band. The sensing element can then be used to damp one of the two dipoles, varying the performance of that dipole as it changes in resistance. Here, the damping element was placed on the lower frequency dipole. Depending on the target resistance range and the difference in target frequencies of the two dipoles, sensing can be achieved either by shifting the resonant frequency of the tag or by comparing the damping between the two dipoles. These two sensing modes are described below and the simulations presented were performed using Ansys HFSS.

2.1 Sensing by Peak Shift

When the resistance of the sensing element is low, or if the target frequencies are sufficiently close, the two resonant peaks of the antenna merge into one. The relative amplitude of the two resonant peaks dictate the resultant peak frequency. The relative amplitudes of resonant peaks can be changed by the damping element, decreasing the influence of the damped dipole on the resultant resonant peak. This effect can be seen in Figure 2-3. As the resistance of the sensing element decreases, the damping of the lower frequency dipole increases, and the resultant peak shifts up in frequency. We also notice that there is a fairly linear relationship between the resistance and resonant frequency. This relationship only holds within a certain operating range, as the peak will not shift past the higher frequency dipole, and too high of a resistance will change the shape of the response altogether.

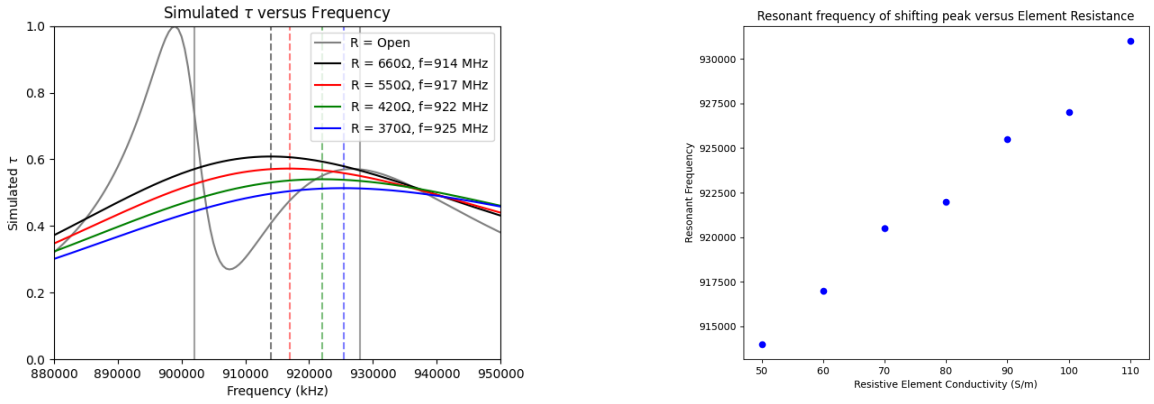

(a) Shifting resonant frequency by varying sensing element resistance. As the resistance decreases, the resultant peak shifts upwards.Upper and lower bounds of UHF band shown in gray.

(b) There is a mostly linear relationship between the element resistance and the resulting resonant frequency, and the error seen is likely due to numerical error in simulation.

Figure 2-3: Performance of sensing by resonant peak shifting

2.2 Sensing by Relative Damping

With higher resistance sensing elements or with target frequencies farther apart, the proposed antenna design can also operate in a regime where the peaks remain distinct in the tag's frequency response. In this regime, τ at the upper end of the frequency band remains relatively unchanged, while τ at the low end of the frequency band, where the damping takes place, varies. Note that this design can accommodate a wide range of sensing element resistances, as either of the peaks can be moved closer or farther from the frequency band, raising or lowering their effective τ before any damping takes place. The response in this range of operation can be seen in Figure 2-4.

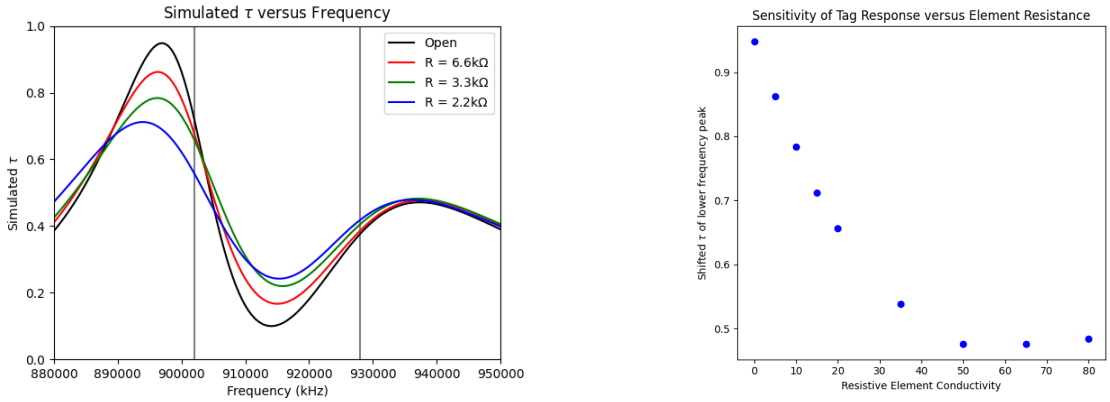

(a) Damping the lower frequency peak, while using the higher frequency peak as a reference. As resistance decreases, damping increases and τ at lower frequencies decreases. Upper and lower bounds of UHF band shown in gray.

(b) We notice that in a specific conductivity range, corresponding to a resistance range, the tag is sensitive to changes in resistance. As the conductivity increases outside of the target range τ becomes less sensitive to changes in resistance

Figure 2-4: Performance of sensing by relative damping

Chapter 3

Fabrication and Testing protocols

3.1 RFID Tag Fabrication

To determine the tag dimensions, seen in Table 3.1, the tag was considered as having four components: the IC, strap (which helps attach the IC to the antenna), antenna, and substrate. The material properties of the antenna and substrate are well known and can be used in simulations. The IC selected is the NXP UCODE7, with a listed complex impedance of $12.5 - j277\Omega$ to $13.5 - j195\Omega$ at 915MHz depending on its mounting to the antenna [17]. In order to narrow this range, as well as to include the strap in the lumped impedance, T-match antennas RFID tags as described in [18], with similar IC mounting to our RFID tags, were fabricated and tested. This resulted in a lumped impedance closer to $Z_c = 12.5 - j250\Omega$. The T-match antenna was selected due to its low number of dimensional parameters and well-characterized performance.

With this impedance, the tag was designed so that the lower frequency dipole is impedance matched with the IC.This can be seen with a τ close to 1 in Figure 2-4, as well as the Smith Chart in Figure 3-1, when the sensing element is not present. While sacrificing some perfor-

Dimension	a	b	c	d	Trace Width	Gap Width
Value (mm)	11	38	16	39.5	1.6	1

Table 3.1: Dimensions used for prototype tag.

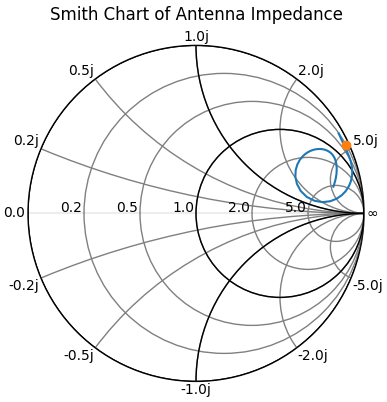

Figure 3-1: Smith chart of antenna impedance, shown in blue, over the frequency range. Complex conjugate of chip impedance at 915MHz shown in orange, and matching is close.

mance of the higher frequency dipole, this matching allows for the widest range of τ variation due to changes in the sensing element, allowing the widest range of resistance values to be sensed.

Having determined the target dimensions, prototype tags (Fig. 3-2) were constructed using copper foil (0.038mm thick) backed by a conductive acrylic adhesive (0.038mm thick) on a Kapton polyamide substrate (0.076mm thick). The foil was applied to the substrate, then the antenna shape was cut out using a Silhouette Cameo 4 vinyl cutter, and the unwanted foil was removed. The NXP UCODE7, along with the strap used to attach it to an antenna, were taken from an Avery Dennison 600533 RFID tags. The IC and strap assembly was peeled away from the commercial antenna and then washed with acetone to remove any remaining adhesive. The strap and IC assembly could then be attached to the prototype antenna using anisotropically conducting film tape (ACF, 3M 9703).

To emulate changes in the tag's RF behavior due to the presence of a chemiresistive sensing element, a SMD resistors (0805 size) were attached to the tag at the locations shown in blue in Figure 2-2 using the ACF tape mentioned above. The tag was then placed on a lab bench facing the reader antenna at a given distance and interrogated, as shown in Figure 3-2.

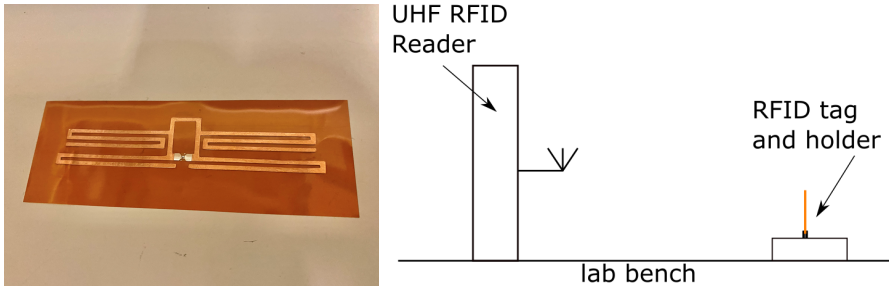

Figure 3-2: Prototype tag constructed from copper foil on Kapton substrate; IC and strap were attached with ACF tape.

3.2 RFID Reader Interrogation Protocol

The IC impedance Z_c is typically listed in the IC datasheet as the impedance at the turn-on threshold power of the chip. As a result, characterization of the tag performance, if relying on Z_c, must always occur at, or close to, the tag's threshold power. Additionally, UHF RFID readers are required to frequency hop over different bands at given time intervals, as mandated by the US FCC regulations [19] to prevent the jamming of channels.

The prototype tags were interrogated using a ThingMagic Sargas 2-Port UHF Reader with the MTI MT-242025/TRH/A (RHCP) antenna. In order to comply with the outlined requirements, a Python wrapper [20] for the Mercury API that interfaces with the reader was used to explicitly control the reader power and frequency. The reader increments the power transmitted while performing a frequency sweep at each power level. To reduce noise, multiple successful readings of the tag are required at each power and frequency. Once the tag successfully responds at a given frequency, the threshold read power P_{th} is noted, and the effective τ_e is calculated using (3.1). The range of τ_e values can then be normalized to the maximum valued reading, resulting in a series of values between 0 and 1.

$$\tau_e \sim \frac{P_{c,\text{threshold}}}{P_{th}} \tag{3.1}$$

The resolution in power and frequency are selected minimize the interrogation time while still extracting the desired information. In this work, incrementing the power by 0.05dBm steps, and the frequency at 1MHz intervals provided the necessary resolution.

Chapter 4

RFID Tag Experimental Results

For the experiments in this thesis, we used the relative damping sensing method. This is because the antenna is easier to tune experimentally, as any change in response can always be seen within the 902MHz to 928MHz window.

4.1 Measurements at Varying Distance

Measurements were taken at 25cm intervals between 1 and 2 meters. Below the 1m distance, between 50cm and 75cm, near field effects begin to influence the response of the tag. Past the 2m distance, because some frequencies have a low τ, full characterization of the tag was not possible. It is important to note, however, that the tag is still functional past 2m, as a response is not needed at all frequencies to extract a reading. Based on an undamped maximum read distance of 6.8m, and the relative power required at the lower distances, the maximum operating distance is estimated to be in the 3m to 4m range.

For each resistance, τ_e was found and then shifted such that the average of the 25% highest frequencies is at $\tau_e = 0$. This was done for visualization purposes, using the higher frequency τ_e values as a reference. We notice that with no resistor in place, τ_e is highest at the lower end of the frequency band. As predicted by the simulations, adding a resistor to the corresponding dipole reduces its τ_e by varying amounts. Shown in Figure 4-1 are the

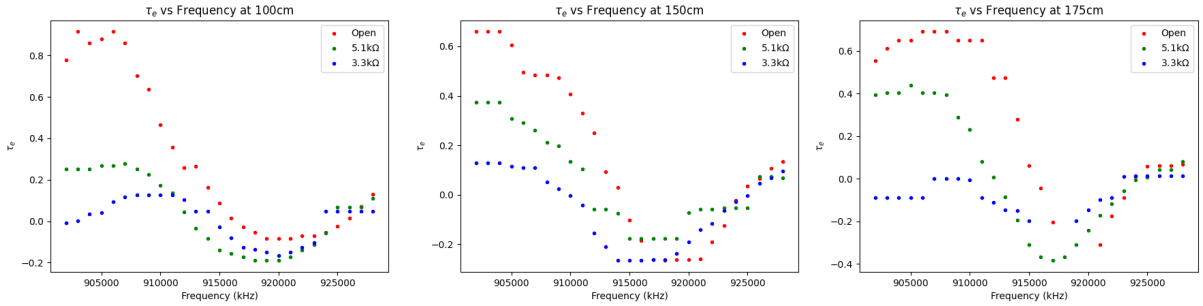

(a) (b) (c)

Figure 4-1: Measurements of τ_e at 100cm, 150cm, and 175cm with no damping, 5.1kΩ, and 3.3kΩ resistors.

1m, 1.5m, and 1.75m readings, that the measurements for each resistance are distinguishable and in agreement with the simulations.

4.2 Measurement Confidence

Due to the noisy nature of the passive RFID system, several samples of the tag were taken for each experiment. Assuming that the measurement noise can be modeled as a Gaussian distribution and that our belief of P_{th}, at a given frequency, can also be modeled as Gaussian distribution, a Gaussian belief update can be used to increase our confidence as the number of samples increases, using the following expressions,

$$\mu_{post} = \frac{\sigma^2_{meas}\mu_{prior} + \mu_{meas}\sigma^2_{prior}}{\sigma^2_{meas} + \sigma^2_{prior}} \ , \tag{4.1}$$

$$\sigma^2_{post} = \frac{\sigma^2_{meas}\sigma^2_{prior}}{\sigma^2_{meas} + \sigma^2_{prior}} \tag{4.2}$$

Where $\mu_{prior}, \sigma^2_{prior}$ are the pre-measurement belief mean and variance of P_{th}, $\mu_{meas}, \sigma^2_{meas}$ are the measurement process mean and variance, and $\mu_{post}, \sigma^2_{post}$ are the updated belief mean and variance.

It is important to note that the variance of the measurement is unknown a-priori. Here,

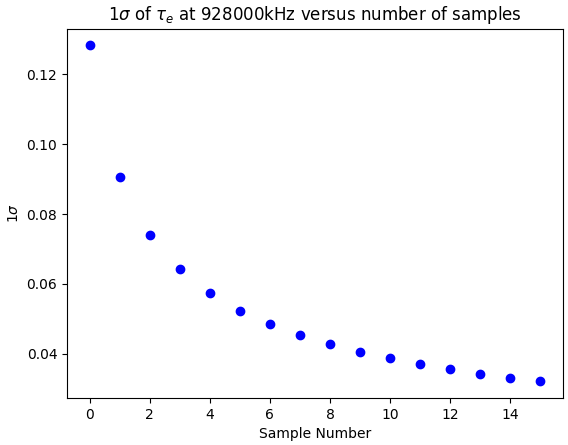

Figure 4-2: Decreasing σ of the measurement belief with increased sampling.

it was estimated by taking measurements of the tag beforehand. This estimated variance was then used for future updates. Using this method, we can see how the belief confidence increases, or σ_{post} decreases, with sample number as shown in Figure 4-2.

4.3 Classification Confidence

Given a measurement, mapping of that measurement to a resistance, or classifying it into a resistance range, must also account for uncertainty. One possible approach would be curve matching with previous data, or to include crude models of the environment. A simpler approach is to use a Naive Bayesian classifier. By considering readings at all distances of a given resistance, we can look at the variance of the measurement assuming the measurements are independent of distance. This is shown in Figure 4-3. It is important to note, however, that the variance of the data set at different distances is higher than at a fixed distance by a factor of about 4. This means that varying distance yields a larger uncertainty, possibly due to a changing environment.

Using a Naive Bayesian classifier, with a uniform, or no, prior belief, we can compare the likelihood of a vector C containing a measurement at the frequencies of interest, given each of the possible resistance values R_i. The likelihood of each resistance can then be calculated

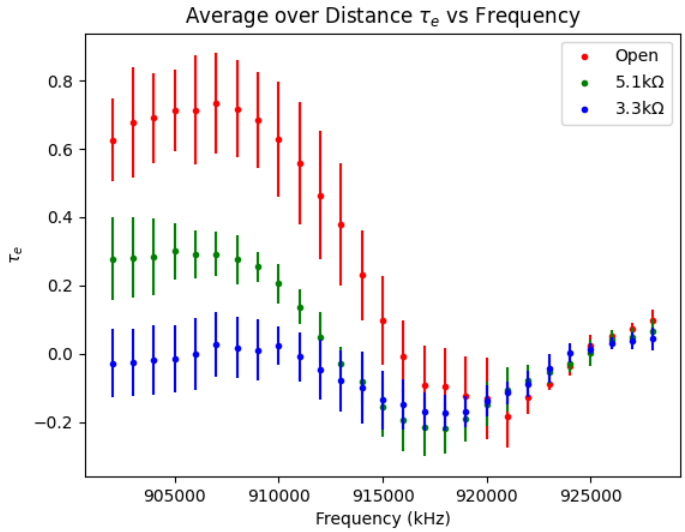

Figure 4-3: τ_e with 1σ error bars of data grouped by distance.

and normalized such that the probabilities of all resistances add up to 1. This approach allows for classification of a measurement into discrete resistances and can be seen in (4.3).

$$P(r = R_i|\bar{\mathbf{C}}) = \frac{P(\bar{\mathbf{C}}|r = R_i)}{\sum P(\bar{\mathbf{C}}|R_i)} \tag{4.3}$$

4.4 Discussion

The prototype tag design was presented as a proof of concept of a sensing tag that functions over a range of distances. If the resistance and change in resistance are well defined for specific applications, the antenna could be optimized to have a τ closer to 1 for the higher frequency dipole.

The Gaussian distribution framework allows the tag to be used, either for sensing continuous changes in the sensing element properties or, for detecting larger, binary changes in properties. In the first case, it will likely require a larger number of samples, while in the latter case, one could sample only the lower and higher frequencies in the band to extract a measurement. This would result in faster read times at a small cost in confidence or resolution.

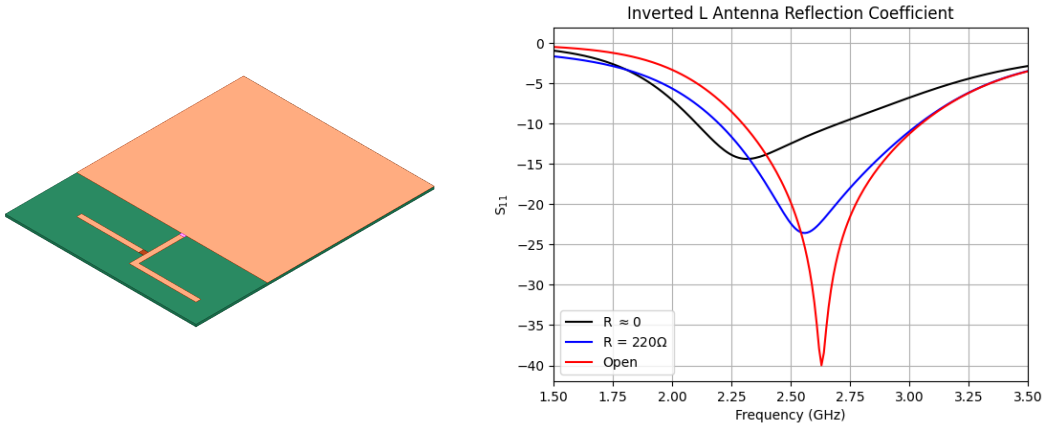

Figure 4-4: Inverted L Antenna and S_{11} for varying resistive element

The proposed approach could be extended to integrate two sensing modes into one tag. One sensing element would act as those used in this work, while another would be added in series or parallel with Z_a, damping the entire response of the tag. This would allow, if at a fixed distance, decoupling of the two sensors by sensing both the RSSI at all frequencies as well as changes response in the frequency domain, when operating at a fixed distance.

This approach could also be used for other applications, including tuning of powered RF devices or other types of RFID tags. Inexpensive RF devices, where a finely tuned resonant frequency is needed, may require the tuning of a capacitive or inductive element [21], but with the approach described in this thesis, they could be tuned using resistive elements instead. Additionally, this antenna design can also be used to effectively increase the bandwidth of an antenna. Show in Figure 4-4 is our approach used with an inverted L PCB antenna. The performance of the traditional inverted L antenna can be seen in red. As the resistance of the resistive element decreases, the curve shifts towards the black trace. This both increases the performance in the lower frequency range as well as shifts the resonant peak downwards.

Chapter 5

Chemiresistive CNT-Based RFID Tags

5.1 CNT Ink Formulation

Viable CNT inks require a homogenous dispersion of the CNTs in the solvent to ensure repeatability during deposition. The high aspect ratio and flexibility of CNTs, along with van der Waals forces, often result in aggregation of the CNTs into bundles [22]. One way to combat this aggregation is through the use of surfactants such as sodium dodecylbenzene-sulfonate (SDBS), Triton X-100, or other polymers. Various solvents can also influence the stability of CNT suspensions [23]. As a result, CNT inks can vary in stability, concentration, and drying time once deposited. It is also important to note that during drying after deposition, the effective concentration of CNTs increases and often results in aggregation.

The requirements for the CNT inks in this work were a concentration of ≥ 0.01mg/mL due to bulk conductivity requirements, compatibility with the Co(tpfpp)ClO_4 metal complex functionalization presented in [24, 25] along with a high semiconducting CNT content, and stability throughout the drying process after deposition.

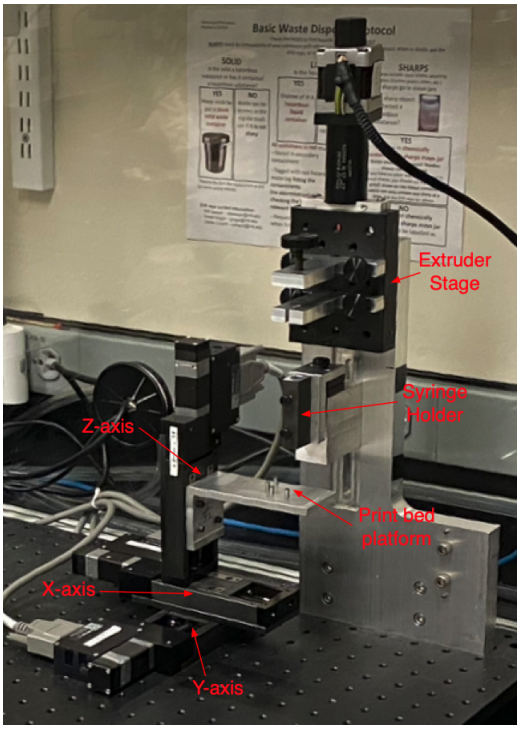

Figure 5-1: Picture of CNT printer, shown in red are the three movement axes, extruder axis, print bed, and syringe holder.

5.2 Printing System and Methods

In order to repeatably deposit the CNT inks, a direct-write printer was built. The motion system of the printer uses Zaber LRM025A-E03T3 linear stages and has an accuracy of 8μm and repeatability of $< 4\mu$m, along with a travel distance of 25mm along each axis. The extrusion system consists of a Hamilton 7656-01 syringe and a displacement-based extruder using the Physik Instrumente M-229.26S, with a minimum incremental movement of 1μm. The displacement method was chosen over a pressure-based approach in order to accommodate a wide range of ink viscosities and needle dimensions. A python script and the corresponding API for each stage was used to control the printer, which can be seen in Figure 5-1. Using a needle with an inner diameter of 168μm, the meniscus at the end of the needle, shown in Figure 5-2, could be used to produce dots down to 121μm in diameter, using approximately 1.6nL of ink per dot. Features of this size proved to be sufficiently small to print resistive elements for the experimental RFID tags.

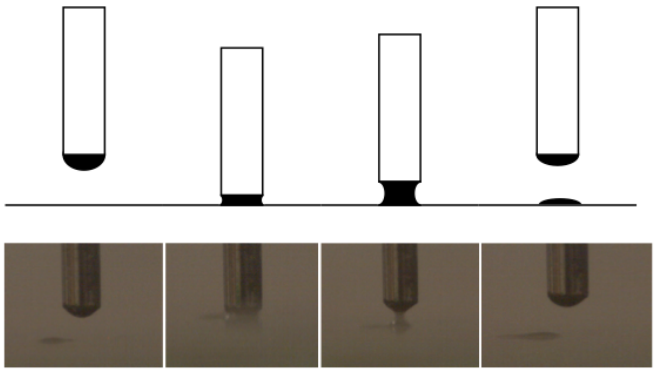

Figure 5-2: Diagrams and pictures of printing with meniscus. Syringe extrudes to grow the meniscus, which is then touched down, and separates to break the capillary bridge, depositing ink. Note that no extrusion takes place during contact.

5.3 CNT Printing Results

Figure 5-3 shows images of sample prints from four of the tested inks, including Tuball Coat-E, Sigma Aldrich $(6, 5)$ CNT suspensions, and Nanointegris IsoSol-S100. The first Sigma Alrich CNT suspension was made by adding 50mg poly(4-vinylpyridine) (P4VP) and 5mg CNT powder to 10mL N,N-dimethylformamide (DMF), followed by sonication in a bath for 2 hours and centrifuging at 3000RPM for 3 hours to remove any remaining clusters. A suspension without surfactant was made as well, with 5mg CNT powder in 10mL 1,2-diclorobenzene (ODCB), followed by the same sonication and centrifuging. The Tuball Coat-E ink, while having a relatively high concentration of CNTs at 0.4mg/mL, also contains a large amount of surfactant and the regular 66% semiconducting CNTs, making the $Co(tpfpp)ClO_4$ functionalization ineffective in our testing. Both the Sigma Alrich semiconducting enhanced powder suspensions, with 95% of the CNTs being semiconducting, were not stable enough during drying as can be seen by the aggregation of bundles. The NanoInegris IsoSol-S100 ink performed the best, with a concentration of > 0.01mg/mL, $> 99.9\%$ semiconducting CNTs, and stability during drying.

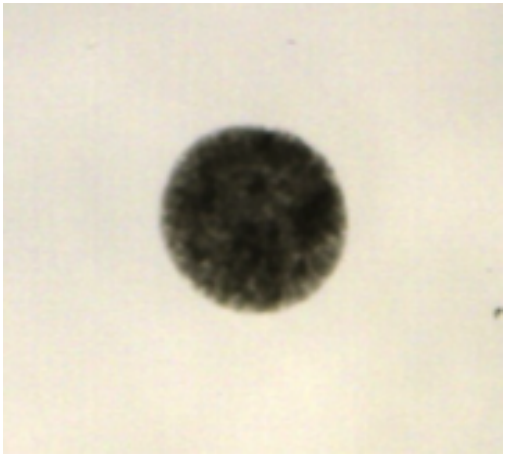

(a) Tuball Coat-E shows stability during drying, seen by the uniform dot.

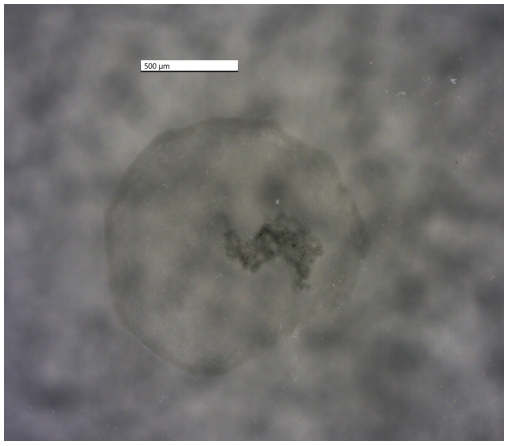

(b) Sigma Aldrich CNTs with no surfactant in ODCB aggregate into bundles.

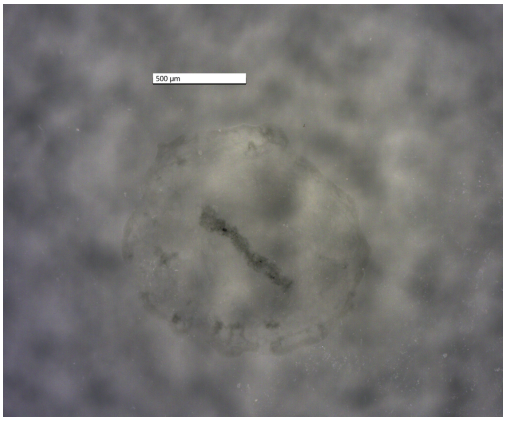

(c) Sigma Aldrich CNTs with P4VP in DMF aggregate into bundles during drying.

(d) Nanointegris IsoSol-S100 creates a relatively uniform dot, despite the coffee ring effect that can be seen.

Figure 5-3: Printed samples of four candidate inks

5.4 CNT Conductivity Range and Sensitivity

The conductivity of the IsoSol-S100 was tested using gold electrodes on a glass substrate, shown in Figure 5-4. A mask was cut from kapton tape and placed over a glass slide substrate after which 15nm of chromium followed by 50nm gold were sputtered on. The electrodes were 1mm wide and with a gap of 0.5mm, and five layers (1mm diameter dot) of IsoSol-S100 were deposited, with an estimated total volume of 8nL. The resulting resistance was around 300kΩ. We noticed that as layers of printed CNTs are stacked, we see a decrease in resistance, which can be explained by the nonlinear trends shown in [26]. This decrease in resistance leads to the conclusion that at this scale, the bulk resistance of the CNT network dominates over the CNT-Au contact resistance. Once the CNT ink had fully dried the same volume of 1mg/mL Co(tpfpp)ClO_4 in dichloromethane (DCM) was added and the resistance dropped to between 10kΩ and 11kΩ, which can likely be attributed to the functionalization p-doping the semiconducting CNTs [27].

The sample was then exposed to 100ppm ammonia (1% NH_3 in N_2, further diluted with air) in a teflon chamber for 15 minutes, followed by flushing of the chamber with air for 25 minutes. The NH_3 flow rate was set to 1L/min and the chamber volume was approximately 5mL, so it is expected that the samples were fully exposed to the gas in well under one minute. The change in conductivity of each of the 3 samples is shown in Figure 5-4. We notice that the maximum change in conductivity is about 80%, which then settles to approximately 65% over the measured time period. Because the volume of the chamber is small compared to the flow rate of the NH_3 and air, we note that the change in resistance over time is due to the intrinsic response of the functionalized CNTs, rather than an increasing concentration of ammonia.

5.5 CNT RFID Tag Results

Two sensing tags were made by first sputtering gold electrodes on the polyamide film located where the SMD resistors were placed on the original prototype tags. CNTs were deposited

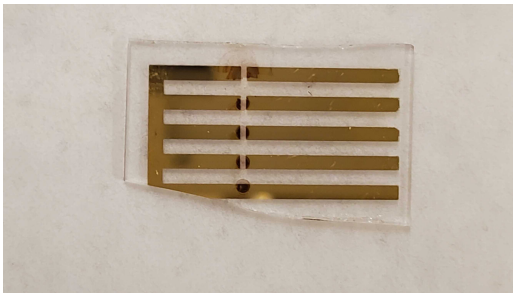

(a) Gold electrode for conductivity testing.

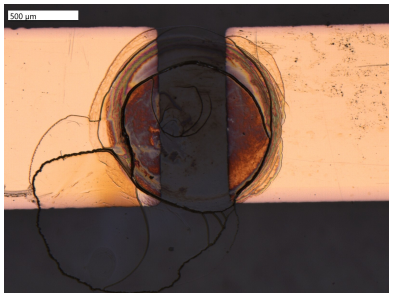

(b) Printed CNT sample on gold electrode

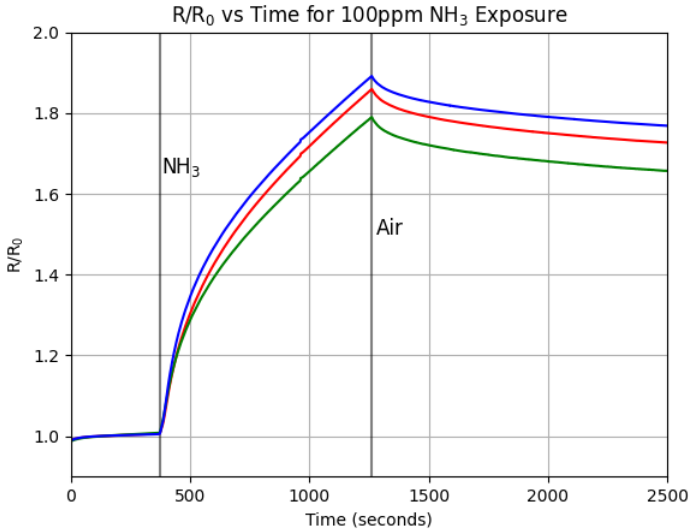

(c) R/R_0 versus time for exposure to NH_3 and air.

Figure 5-4: Electrode for CNT conductivity testing and sensitivity to NH_3.

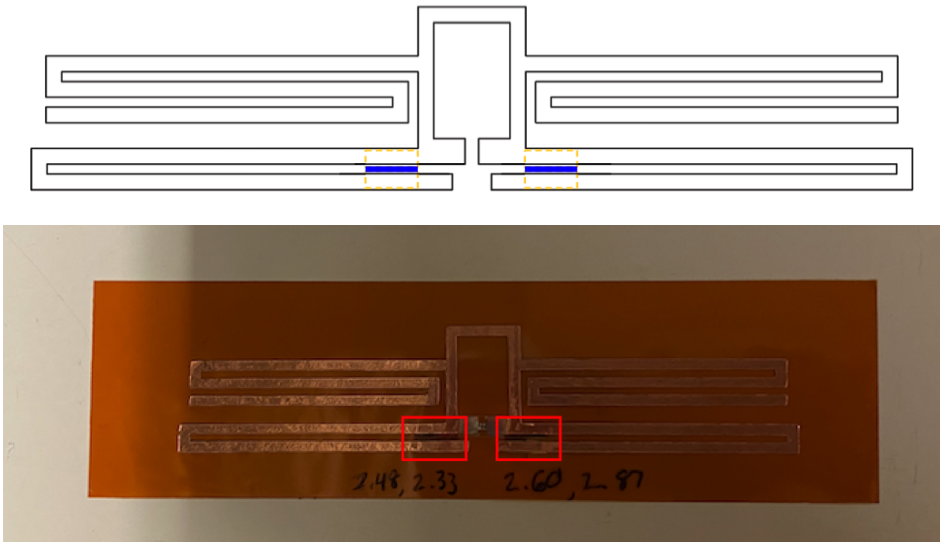

Figure 5-5: Diagram and picture of CNT RFID tag. Diagram shows CNTs in blue on gold electrodes. Picture has sensing element outlined in red

using overlapping 1mm diameter dots to cover the 3mm by 0.2mm gap, followed by the same volume of Co(tpfpp)ClO_4 in DCM. This process was repeated approximately six times until the desired resistance across the electrodes was reached. The sensing element resistances were $2.33k\Omega, 2.61k\Omega$ on the first tag, and $3k\Omega, 3.2k\Omega$ on the second tag.

The copper antenna was then placed over the gold electrodes such that the conductive adhesive was in contact with the gold electrodes. The location of the electrodes with deposited CNTs can be seen in Figure 5-5. The tags were then exposed to 1000ppm NH_3 for 15 minutes. It is expected that the resistive change in CNT resistance increases with increased exposure to ammonia. So, the concentration of NH_3 was selected to maximize the change in resistance while still being considered a trace amount of ammonia. Shown in Figure 5-6 are the results at 100cm for both tags, showing similar performance, and at 200cm for one of the tags, demonstrating functionality at a different distance.

We notice a similar trend in all test, which can be seen between the red and green data in Figure 5-6(d). In all cases, the ammonia exposure increased the resistance of the resistive element, resulting in an increase in τ_e in the lower frequency range. This is in agreement with both the simulations as well as the original SMD resistor prototype tags. In particular,

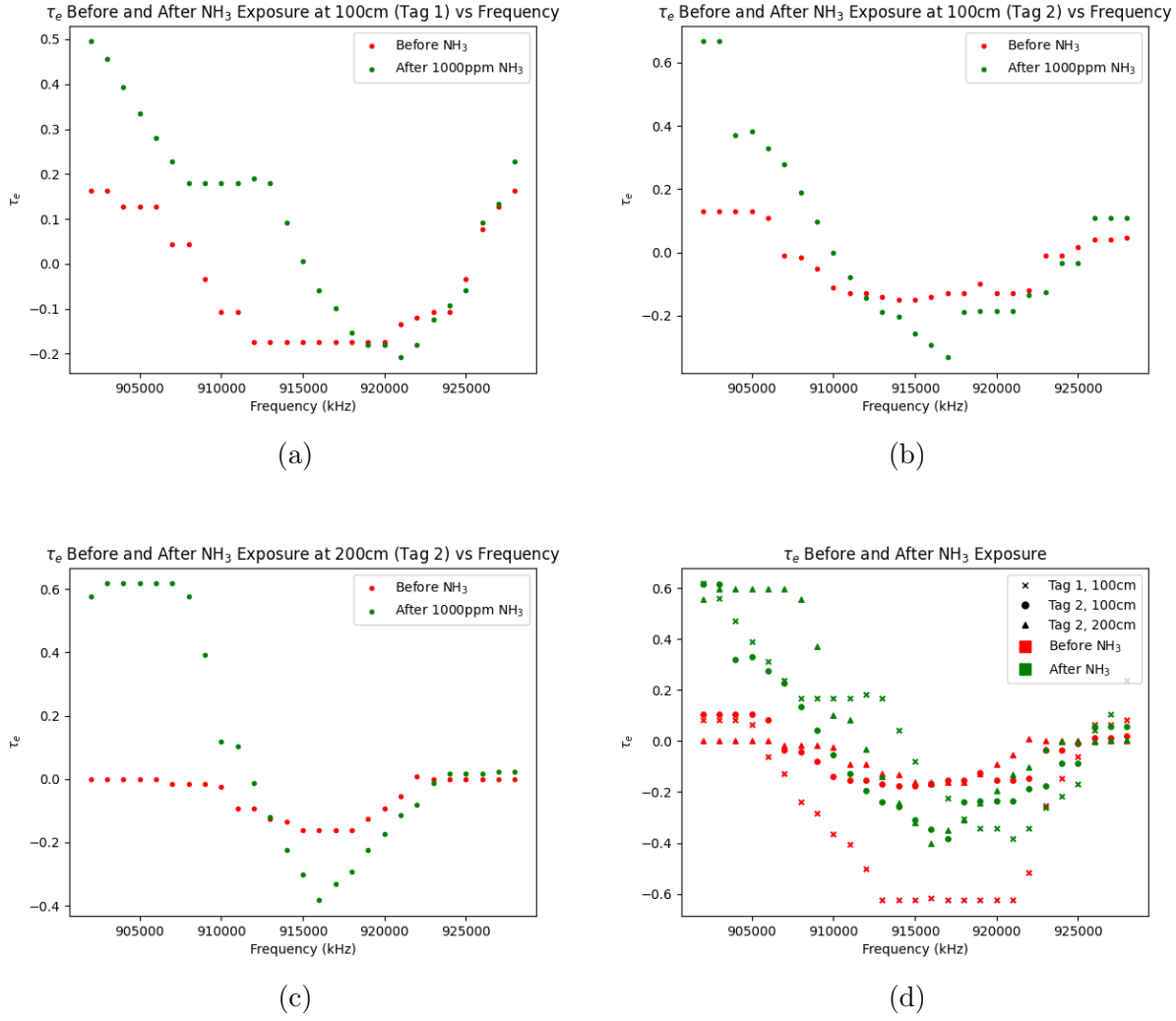

Figure 5-6: Example CNT RFID tag and τ_e experimental results for tags after exposure to NH_3 at 100cm for two different tags, and at 200cm for one of the tags.

we notice that near 902MHz, before exposure, τ_e is around 0 to 0.1. After exposure to NH_3, τ_e shifts up to around 0.6. While copper and other materials present in the tag may react to ammonia, based on the agreement between the CNT RFID tags and the SMD resistor RFID tags, it is expected that the driving factor of the change in response is the CNT sensing element. We also note that the sensitivity of the tag is a function of the confidence required to make a reading. Using the Gaussian belief update approach, with enough interrogations of the tag, we notice that 1σ of our belief of τ_e in our previous experiments is significantly lower than the difference in τ_e we see before and after ammonia exposure here. This leads us to believe that the lower limit of gas detection is below 1000ppm.

Chapter 6

Conclusion and Future Work

This thesis presents a novel design for RF antennas with an application in UHF RFID sensors. By operating in the frequency domain, the proposed RFID tags are able to communicate changes in resistance of a resistive sensing element in a passive, wireless, and inexpensive-to-manufacture manner. While the nature of frequency domain passive RFID sensors results in noisy measurements, Bayesian reasoning is used to determine beliefs as well as allow the tag to operate with varying degrees of confidence and resolution.

This thesis also presents a proof of concept UHF RFID tag that exhibits changes in frequency response from changes in a resistive element on the tag. By varying the relative τ of each dipole of the tag antenna, we could sense 35% changes in resistance. It was also shown that the tag can operate independently of the reader-tag separation distance, albeit with decreased confidence. Sensing tags were also demonstrated to work, exhibiting an irreversible change in response after exposure to 1000ppm NH_3 for 15 minutes.

For future work, there are still open questions in terms of tag performance and manufacturing methods.

- It is important to characterize the bulk resistance of the functionalized CNT networks, according to the type and degree of functionalization, dot overlap, and total number of layers.
- The current fabrication method is functional, but CNTs cannot be printed onto the

copper traces due to the solvent mixing with the adhesive. Future methods to explore include etching the antenna, or using silver conductive inks to screen print the antenna. The scalability of these methods toward commercially relevant quantities can also be assessed.

- Characterization of the CNT RFID tag performance and sensitivity as a function of distance. With this, more complex curve fitting approaches could be explored instead of simply looking at the upper and lower ends of the frequency band. From this, the detection limit can be identified for various chemical analytes of interest.

Bibliography

[1] R. A. Potyrailo, C. Surman, N. Nagraj, and A. Burns, "Materials and transducers toward selective wireless gas sensing," *ACS Publications*, vol. 111, no. 11, 2011.

[2] A. Dada and F. Thiesse, "Sensor applications in the supply chain: The example of quality-based issuing of perishables," in *The Internet of Things*, C. Floerkemeier, M. Langheinrich, E. Fleisch, F. Mattern, and S. E. Sarma, Eds. Berlin, Heidelberg: Springer Berlin Heidelberg, 2008, pp. 140–154.

[3] R. Tang, Y. Shit, Z. Hou, and L. Wei, "Carbon nanotube-based chemiresistive sensors," *Sensors*, vol. 17, no. 4, 2017.

[4] H. Bai and G. Shi, "Gas sensors based on conducting polymers," *Sensors (Basel)*, 2007.

[5] S. Dehghani and M. K. Moravvvej-Farshi, "Temperature dependence of electrical resistance of individual carbon nanotubes and carbon nanotubes network," *Modern Physics Letters B*, vol. 26, 2012.

[6] "Switchable single-walled carbon nanotube–polymer composites for co2 sensing," *ACS Applied Materials and Interfaces*, Bora Yoon and Seon-Jin Choi and Timothy M. Swager and Gary F. Walsh.

[7] R. Bhattacharyya, C. Floerkemeier, and S. Sarma, "Low-cost, ubiquitous rfid-tag-antenna-based sensing," *Proceedings of the IEEE*, vol. 98, 2010.

[8] G. Swamy and S. Sarma, "Manufacturing cost simulations for low cost rfid systems," *Massachusetts Institute of Technology Auto-ID Center*, 2003.

[9] M. Bhattacharya, C.-H. Chu, and T. Mullen, "A comparative analysis of rfid adoption in retail and manufacturing sectors," *IEEE International Conference on RFID*, 2009.

[10] L. Yang, R. Zhang, D. Staiculescu, C. Wong, and M. M. Tentzeris, "A novel conformal rfid-enabled module utilizing inkjet-printed antennas and carbon nanotubes for gas-detection applications," *IEEE Antennas and Wireless Propagation Letters*, vol. 8, 2009.

[11] C. Occhiuzzi, A.Rida, G. Marrocco, and M. M. Tentzeris, "Passive ammonia sensor: Rfid tag integrating carbon nanotubes," *IEEE International Symposium on Antennas and Propagation*, 2011.

[12] J. M. Azzarelli, K. A. Mirica, J. B. Ravnsbæk, and T. M. Swager, "Wireless gas detection with a smartphone via rf communication," *PNAS*, vol. 111, 2014.

[13] P. Sen, S. N. R. Kantareddy, R. Bhattacharyya, S. E. Sarma, and J. E. Siegel, "Low-cost diaper wetness detection using hydrogel-based rfid tags," *IEEE Sensors Journal*, 2019.

[14] A. A. Kutty, L. S. Toni Bjornine and, and L. Ukkonen, "A novel carbon nanotube loaded passive uhf rfid sensor tag with built-in reference for wireless gas sensing," *IEEE Microwave, MTT-S International Symposium*, 2016.

[15] K. V. S. Rao, P. V. Nikitin, and S. F. Lamen, "Impedance matching concepts in rfid transponder design," *Fourth IEEE Workshop on Automatic Identification Advanced Technologies*, 2005.

[16] Impinj, "Rfid tag antenna design, design overview and guidelines," 2017.

[17] N. Semiconductors, "Sl3s1204 ucode 7," 2019.

[18] N. A. Mohammed, K. R. Demarest, and D. D. Deavours, "Analysis and synthesis of uhf rfid antennas using the embedded t-match," *IEEE International Conference on RFID*, 2010.

[19] K. Finkenzeller, *RFID Handbook: Fundamentals and Applications in Contactless Smart Cards and Identification*, 2nd ed. New York: John Wiley and Sons Ltd, 2003.

[20] P. Gotthard, "python-mercuryapi," https://github.com/gotthardp/python-mercuryapi, 2020.

[21] A. Kolsrud, M.-Y. Li, and K. Chang, "Frequency tunable cpw-fed cps dipole antenna using varactors," *IEEE Antennas and Propagation Society International Symposium*, 1998.

[22] L. Vaisman, H. D. Wagner, and G. Marom, "The role of surfactants in dispersion of carbon nanotubes," *Advances in Colloid and Interface Science*, 2006.

[23] F. Sabri, M. Zakaria, and H. Akil, "Dispersion and stability of multiwalled carbon nanotubes (mwcnts) in different solvents," *AIP Conference Proceedings 2267*, 2020.

[24] C. Mackin, V. Schroeder, A. Zurutuza, C. Su, J. Kong, T. M. Swager, and T. Palacios, "Chemiresistive graphene sensors for ammonia detection," *Applied Materials and Interfaces*, 2018.

[25] S. F. L. A. R. Petty, G. T. Sazama, and T. M. Swager, "Single-walled carbon nanotube/metalloporphyrin composites for the chemiresistive detection of amines and meat spoilage," *Angewandte Chemie International Edition*, 2015.

[26] R. P. Tortorich and J.-W. Choi, "Inkjet printing of carbon nanotubes," *Nanomaterials*, 2013.

[27] Conversation with Lennon Luo (Swager Group MIT, 2022).